Journal of Energy Storage 15 (2018) 228–244

Contents lists available at ScienceDirect

Journal of Energy Storage

journal homepage: www.elsevier.com/locate/est

Battery cycle life test development for high-performance electric vehicle applications

Quirin Kellner[a,*], Elham Hosseinzadeh[a], Gael Chouchelamane[b], Widanalage Dhammika Widanage[a], James Marco[a]

[a] WMG, University of Warwick, Coventry, CV4 7AL, UK
[b] Jaguar Land Rover, Banbury Road, Warwick, CV35 0XJ, UK

ARTICLE INFO

Article history:
Received 7 June 2017
Received in revised form 23 November 2017
Accepted 23 November 2017
Available online xxx

Keywords:
High-performance
Electric vehicles
Duty cycles
Cycle life testing
Lithium ion batteries

ABSTRACT

High Performance (HP) battery electric vehicle (BEV) and racing applications represent significantly different use cases than those associated with conventional consumer vehicles and road driving. The differences between HP use cases and the duty-cycles embodied within established battery test standards will lead to unrepresentative estimates for battery life and performance within a HP application. A strategic requirement exists to define a methodology that may be used to create a representative HP duty-cycle. Within this paper two methods HP duty-cycle design are evaluated and validated. Extensive simulation results into the electrical performance and heat generation within the battery highlight that the new HP duty-cycles provide a more representative duty-cycle compared to traditional battery test standards. The ability to more accurately predict the performance requirements for the battery system within this emerging and strategically important BEV sector will support a range of engineering functions. In addition, the ability to more accurately define the use-case for a HP-BEV will underpin ongoing experimentation and mathematical modelling to quantify the associated cell ageing and degradation that may occur within HP vehicle applications.

1. Introduction

High Performance (HP) battery electric vehicles (BEV) and electric vehicle (EV) racing applications represent significantly different use cases than those associated with conventional consumer EVs and road driving. Such HP-BEVs are typically driven to the performance limits of the vehicle or the capabilities of the driver. Asus et al. [1,2] conducted extensive tests on a series hybrid racing car to develop a detailed mathematical model of the vehicle that characterised its dynamic behaviour and could underpin drive-cycle prediction. The authors present experimental data, including driver pedal input and system power demands, for the vehicle being driven on the Magny-Cours racing circuit in France. Their analysis highlight significant proportions of time spent at peak demand (full-throttle), in addition to rapid transitions from vehicle acceleration and braking. For a BEV, such a usage profile would translate to extended periods of time when the battery system is under full electrical load for charging or discharging.

By comparing the data presented within [1,2] with that found in studies into urban driving, e.g. [3,4] one of the unique measures of HP driving is not just the high amplitude power demands placed on the vehicle's powertrain, but also the relative time that the vehicle spends at peak-power. In contrast, peak power demand in urban driving is rare, of short duration and interspaced with extended periods of low demand. For HP applications, a complete energy discharge of the battery pack may occur within less than a single hour. Conversely, with a conventional EV it may take many hours or even days to deplete the energy content of the battery pack [5].

International standards and best-practice guides exist that address the performance evaluation requirements for EV lithium ion battery (LIB) systems. Each standard addresses different requirements for performance, robustness and safety and how

Abbreviations: BEV, battery electric vehicle; CDF, cumulative distribution function; C-rate, current rate; DOD, depth of discharge; DST, Dynamic Stress Test; eCDF, empirical cumulative distribution function; ECM, equivalent circuit model; EV, electric vehicle; FFT, fast fourier transform; FTP-75, federal testing procedure; HP, high-performance; HP-BEV, high-performance battery electric vehicle; HP-MSC, high-performance multisine cycle; HP-RPC, high-performance random pulse cycle; iCDF, inverse cumulative distribution function; IECC, IEC 62660-1 cycle life test profile A; LFP, lithium-iron-phosphate; LIB, lithium ion battery; MSC, multisine cycle; OEM, original equipment manufacturer.

* Corresponding author.
E-mail addresses: q.kellner@warwick.ac.uk (Q. Kellner), e.hosseinzadeh@warwick.ac.uk (E. Hosseinzadeh), gchouch3@jaguarlandrover.com (G. Chouchelamane), dhammika.widanalage@warwick.ac.uk (W.D. Widanage), james.marco@warwick.ac.uk (J. Marco).

https://doi.org/10.1016/j.est.2017.11.019

testing should be undertaken at either a cell (i.e. IEC 62660-1 [6]), module (i.e. ISO 12405-2 [7]) or system level (i.e. Department of Energy battery test manual for electric vehicles [8]). Within [8] the Dynamic Stress Test (DST) is a simplified version of the electrical loading associated with a EV traversing the Federal Testing Procedure (FTP-75) drive-cycle [9]. The ISO and IEC standards contain comparable duty-cycles that are often employed by vehicle original equipment manufacturers (OEMs) and system suppliers for component selection and battery system evaluation. However, as reported within [10,11], the underpinning drive-cycles that are used as the basis for the design of the battery load-profile are known to be unrepresentative of a number of different vehicle types, driving styles and environmental conditions. The authors assert that the differences between HP and standardised duty-cycle profiles are likely to influence performance requirements of the battery systems and the rate of degradation that may occur within the cells that comprise the HP vehicle battery system.

Although the causality between cell degradation and the external environment and electrical load is known to vary considerably between different cell types, chemistries and form factors, there is a range of common ageing mechanisms that underpin many degradation modes for a variety of LIB chemistries. The topic of LIB degradation and associated ageing mechanisms is the subject of considerable academic and industrial research [12–16] and therefore a full explanation will not be repeated. For completeness, Table 1 summarises those key ageing factors that are most pertinent to this study. Given the increased intensity of ageing mechanisms such as electrical current and cell operating temperature associated with HP driving or EV racing, it is expected that the performance requirements and degradation profile of batteries employed within HP applications may not correspond well with experimental results from standardised tests and from existing research that is focussed on consumer BEVs and urban driving.

To progress the research into better understanding the performance requirements and cell degradation models associated with HP-BEV use, the first strategic requirement is to define a methodology that may be used to define a representative duty-cycle that, in turn, can be used to underpin subsequent experimentation and mathematical modelling.

This paper is structured as follows. Section 2 presents two methods of duty-cycle design. The first, extends the traditional process employed for drive-cycle construction within the time domain. The second exploits recent innovations in battery test case design within the frequency domain. Within Sections 3 and 4 the new duty-cycles are evaluated through three case studies that firstly compare the new HP duty-cycles against the battery power demand for a real-world race-circuit. Secondly, results are presented that quantify the differences in performance requirements for the battery based on HP duty-cycles compared to traditional test standards. Finally, results from a thermal modelling simulation are reported that highlight the level of heat generation within the battery under HP-BEV applications and compares this to that predicted using established battery test methods. Conclusions from this research are presented in Section 5.

2. Methods for duty-cycle development

One existing area of research engaged in the development of testing profiles that preserve traits in the source data is that of driving cycle design. The underlying principle of driving cycle construction is to develop a cycle whose properties match specific criteria extracted from a database. As such, the methods explored in this field lend themselves to the construction of HP duty-cycles.

Another approach to duty-cycle design is to construct the HP duty-cycle based on a desired amplitude spectrum and inverse cumulative distribution function (iCDF) [24]. The amplitude spectrum of a duty-cycle is its representation in the frequency domain and thus contains information of the amplitudes and frequencies that the battery would be subject to. The iCDF is the mathematical representation of a cumulative histogram and describes how much time is spent within each amplitude range. Recent publications by Widanage et al. have shown that the consideration of target amplitude spectra during characterization tests can positively affect the representativeness of testing procedures [25,26], while concurrently reducing the time required to undertake the experimental evaluation. This research describes a method for superimposing the Pulse Power Current (PPC) test profile as described in the IEC 62660-1 standard [6] with a multisine signal. The result is a charge sustaining test-profile called a pulse-multisine which approximates the amplitude spectrum of a duty-cycle derived from a driving cycle. Within [26], the pulse-multisine was successfully employed to characterise a number of different cell-types and provide the necessary dataset to parameterise an equivalent circuit model (ECM) representation of the cells. The research highlights that the validation accuracy of the ECM improved when estimated with the pulse-multisine as compared to characterisation tests undertaken in accordance with established methods in [6]. The improved accuracy was attributed to the ability of the pulse multisine to better emulate the frequency bandwidth and amplitude of the electrical loading experienced by the battery system throughout the target drive-cycle. A similar improvement in HP degradation and modelling is therefore expected by designing a HP duty cycle with the appropriate frequency bandwidth and histogram that represent a HP duty cycle database.

Table 1
Duty-cycle conditions and resulting degradation pathways.

Cause/Aggravating factor	Affects	Causes	Ref
High Current	Anode	Lithium plating during charging, especially at high state of charge (SOC) and subsequent solid-electrolyte interface (SEI) growth at locations where lithium metal is exposed to electrolyte	[13,17,18]
		Volume changes resulting in contact loss of active material particles and particle cracking, exposing fresh graphite to the electrolyte and subsequently further SEI growth	[13,17]
	Cathode	Volume changes, and tensile and compressive stresses causing particle cracking	[19,20]
High Temperature	Anode	Decomposition of electrolyte resulting in gassing and further SEI growth	[13,16,17,21]
		Increased rate of parasitic side reactions which includes SEI growth	[13]
		Decomposition of binder causing mechanical instability	[13]
	Cathode	Decomposition of electrolyte resulting in gassing	[17,22,23]
		Increase in phase changes in active material	[17]
		Dissolution of transition metal which may result in material phase change, and its re-deposition on anode	[13,16,17,19]
High Depth of Discharge (DOD)	Anode	Volume changes causing mechanical stresses and particle cracking with subsequent SEI growth	[13]
	Cathode	Volume changes causing mechanical stresses	[13,17]
		Crystal structure disorder causing particle cracking	[17]

The following sub-sections discuss, in greater detail, the creation of a database that defines a range of HP duty-cycles that are deemed to be representative of the real-world use of this form of niche BEV. Based on this database, the two methods of duty-cycle creation, a HP Random Pulse Cycle and a HP Multisine Cycle, are further explained and evaluated.

2.1. Duty-cycle database

To quantify the target criteria that will underpin the design of both duty-cycles, a database of representative real-world HP duty-cycles is required from which key performance measures can be extracted. Ideally, this data-set would comprise actual vehicle data recorded over a range of different race circuits. However, due to obvious financial and logistical challenges associated with obtaining this data, it was decided to employ the commercially available simulation software IPG CarMaker to simulate the race circuits, the HP-BEV and the driver to generate the required data. The fundamental process employed is similar to that presented within [27]. It is beyond the scope of this paper to present the full derivation and validation of the mathematical models that comprise the race circuits, the HP-BEV and Driver. This information is published within [28–30] and will therefore not be repeated. However, for completeness, a summary of the pertinent aspects of the methodology are provided.

A total of eleven internationally recognised race circuits were modelled as part of creating the database using the same process as described within [27].

The vehicle model employed within this work is based on the Audi R8 demonstration vehicle that is made available within the IPG CarMaker software. Key vehicle subsystems such as the suspension, hydraulic brakes steering and tire models were unchanged. Rolling resistance on an individual wheel is calculated within the simulation suite as a torque acting along the wheel spin axis, according to Eq. (1), where T_{RR} is the tire rolling resistance Torque, N is the normal Force at the tyre contact point, k_{rr} is the coefficient of rolling resistance r is the radius of the loaded wheel, v is the velocity of the tire belt at the tire-road contact point.

$$T_{RR} = -|N * k_{rr}| * r * sgn(v) \tag{1}$$

$$sgn\ (v) = 1, 0, -1;\ for\ v > 0, v = 0, v < 0 \tag{2}$$

The longitudinal drag coefficient was increased from 0.2 to 0.3. This was to ensure that the value was more representative of realistic values [31]. The powertrain model of the demonstration vehicle was replaced with a representative HP-BEV drivetrain, comprising two electrical machines, each mechanically coupled through an automated gearbox with two gears and differential to the front and rear axles respectively. Energy efficiency maps for both, acceleration and regenerative braking for the machine-inverter assemblies were based on real-world test data from commercially available systems. Energy efficiency, defined as the ratio of shaft power to the electrical input power of the inverter was quantified as a function of machine speed and torque. A sequential regenerative braking strategy was implemented, where mechanical brakes are only in use for braking torques which exceed the electric motors' capability. The complete set of model parameters for the HP-BEV are provided in Table 2.

For Driver parameterisation, a racing-circuit driving simulation procedure was executed and the driver aggressiveness (tuneable with respect to both, lateral and longitudinal dynamics) was optimised within the constraints of vehicle adhesion to iteratively improve lap times over each circuit. The final driver settings were subsequently employed for all simulations. Each simulation lasted 1800s to ensure the recorded power demand profile contains the profile for at least one complete lap without a start from standstill for each racing-circuit.

Table 2
Vehicle model parameters.

Parameter	Value
Vehicle body	Rigid body
Vehicle mass	1564 kg
Combined motor power	300 kW
Combined motor torque	850 Nm
Height of center of gravity	0.5 m
Wheelbase	2.67 m
Drag coefficient	0.3
Effective frontal area	2.0 m
Gearing ratio 1st gear	1.4: 1
Gearing ratio 2nd gear	0.45: 1
Final drive gear ratio	5.8: 1
Tire rolling resistance k_{rr}	0.01
Tire friction coefficient μ_r	1
Tire radius r	0.27 m
Axle power split	50–50
0–100 km/h	3.8 s
0–200 km/h	12.4 s
Top speed (km/h)	300 km/h

Table 3 provides, for each race-circuit, a summary of actual vs simulated racing-circuit distance, the associated percentage error in racing-circuit length, the average speed, average of the absolute power, average discharge power after considering regenerative braking, rms power, and peak power when modelled within the CarMaker software.

The peak power demand for each driving scenario is limited by the vehicle capability, reaching a maximum of 300 kW. An example of the vehicle velocity as a function of the driving path as recorded from the simulation for the Silverstone race-circuit is shown in Fig. 1. The corresponding battery pack power demand is shown in Fig. 2a. As expected the vehicle reaches peak velocity on straight stretches of road, and slows down for cornering.

The number and individual periods for each racing-circuit are determined using an unbiased auto-correlation as defined in [32], a step illustrated in Fig. 2b. A duty-cycle for a specific racing-circuit is then approximated as the normalised profile of an average (over the periods) lap ($R(t)$) (Fig. 2c).

Normalisation of the power demand profiles with Eq. (3) allows decoupling the power demand profile from battery parameters with the resulting profiles containing values between −100% and 100%. P_{Norm} is the normalised power, P_{Cycle} is the power demand profile resulting from the simulation, and $\max(P_{System})$ is the peak power that the system can supply to the electric machines. The resulting profiles, although dimensionless, are still fully dependent on the specific properties of the vehicle and driver models, and race-circuit selection. As such, the normalized profiles relay information about their intensity as a function of the system's peak capability, without eliminating crucial information about differences between individual duty-cycles.

$$P_{Norm} = \frac{P_{Cycle}}{\max(P_{System})} \tag{3}$$

This processing step also allows direct comparison with the battery testing profiles in ISO 12405-2, IEC 62620-1 and Battery Test Manual [6–8]. Visual inspection of Fig. 2c and d reveals large differences between a HP application duty-cycle and the cycle life testing profile A as found in the IEC 62660-1 standard, namely the frequency of changes between charging and discharging, time spent at high charging and discharging levels, level of charging and

Table 3
Racing-circuit model and simulation result overview.

Racing-circuit	Model length (km)	Official length (km)	Delta (%)	Average speed (m/s)	Average absolute Power (kW)	Average Power (kW)	RMS Power (kW)	Peak discharge power (kW)
Dunsfold Park (Top Gear)	2.852	2.818	1.22	33.05	137.8	55.8	167.3	300
Anglesey International Circuit	3.294	3.381	−2.57	29.02	118.4	43.6	148.1	300
Goodwood Full Circuit	3.853	3.832	0.55	42.44	153.0	77.5	186.4	300
Brands Hatch Grand Prix Circuit	3.908	3.917	−0.23	33.96	135.9	53.2	166.3	300
Magny Cours GP	4.436	4.411	0.57	34.51	161.0	68.4	192.3	300
Lausitzring Automobilsport	4.551	4.534	0.37	31.89	132.9	52.8	164.7	300
Nürburgring GP	5.142	5.148	−0.12	32.58	138.0	59.3	168.5	300
Suzuka GP	5.828	5.807	0.36	33.02	139.2	60.6	169.7	300
Silverstone GP	5.92	5.892	0.46	35.94	143.3	59.8	173.6	300
Le Mans Circuit de la Sarthe	13.626	13.629	−0.02	44.91	201.3	109.9	228.1	300
Nürburgring Nordschleife (with altitude)	20.56	20.832	1.31	40.82	145.5	75.8	178.9	300
Nürburgring Nordschleife	20.8	20.832	−0.15	39.93	142.7	76.0	176.6	300

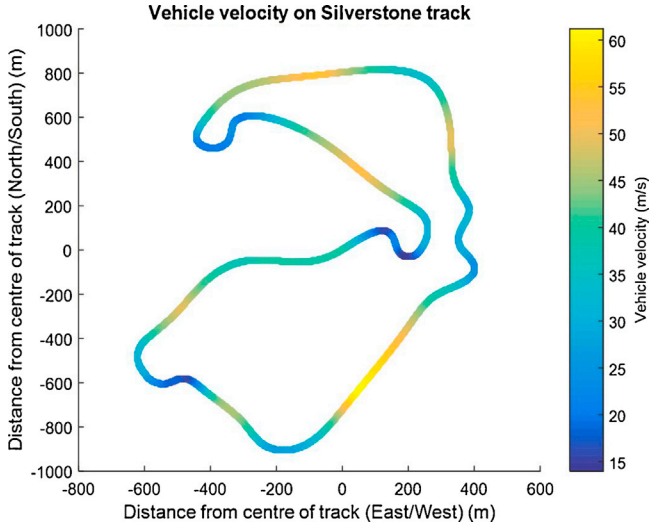

Fig. 1. Vehicle velocity as a function of driving path on Silverstone race-circuit.

discharging power and duration; further strengthening the arguments for a bespoke HP duty-cycle.

2.2. Method one: HP random pulse cycle

The typical process employed within the literature for drive-cycle design is as follows. A database of driving conditions is created and subsequently divided into smaller segments (based on time or stopping segments), often referred to as micro-trips [33]. Concatenating the individual segments together, either through a random process or via stochastic selection yields the final drive-cycle. Optimisation methods are often employed to ensure that the resulting drive-cycle meets the target criteria selected [34]. Common measures where a correlation is required include: average speed, duration, acceleration, idle time, and speed-acceleration frequency distribution (SAFD) [35–41]. The selection of which criteria to employ within the cost-function of the optimisation process is known to be key. In order to employ the drive-cycle creation analogy, it is important that target parameters are selected in accordance with their potential influence on battery degradation.

2.2.1. HP target criteria

Cells cycled at higher current rates (C-rates) are known to display reduced cycle life [42,43] which should be reflected in the target criteria. Preliminary results presented within [44] indicate that both, charging and discharging pulses, at peak power cause a higher capacity loss over time than a pulse with the same cumulative energy but lower magnitude. Pulsed profiles also appear to cause more capacity fade than a constant current discharge with the same cumulative discharge energy [45]. Accurate representation of the magnitude and duration of charging and discharging pulses is therefore deemed to be necessary. As the anode and cathode degrade under different ageing mechanisms [13] it is also required to take into account the duration the cell is being charged and discharged respectively to ensure that this is equally represented within the derived HP duty-cycle.

To extract information such as power pulse duration and magnitude from the duty-cycles, the following process was followed. Each race circuit duty-cycle signal ($R(t)$) was divided into a set of duty pulses ($p(t)$), defined as the time signal between two zero crossings. This is similar to the definition of a micro-trip often employed within drive-cycle construction studies [46]. The entire database is broken down into a finite number of duty pulses and expressed as a single set $\mathbb{P}$ with k number of duty pulses in the database.

$$\mathbb{P} = \{p_1(t), p_2(t), p_3(t), \ldots, p_k(t)\} \tag{4}$$

Furthermore, the set $\mathbb{P}$ is broken down into two subsets, D and $\mathbb{C}$ containing all recorded discharging ($d_i(t)$) and charging ($c_i(t)$) pulses, respectively, where i is the i^{th} pulse contained within in each set. The conditions for a pulse of duration L to be classified as a discharging or charging pulse are defined in Eqs. (5) and (6) respectively.

$$p(t) = d(t), for \int_0^L p(t)dt < 0 \tag{5}$$

$$p(t) = c(t), for \int_0^L p(t)dt > 0 \tag{6}$$

As such:

$$\mathbb{P} \supset \mathbb{D}, \mathbb{C} \tag{7}$$

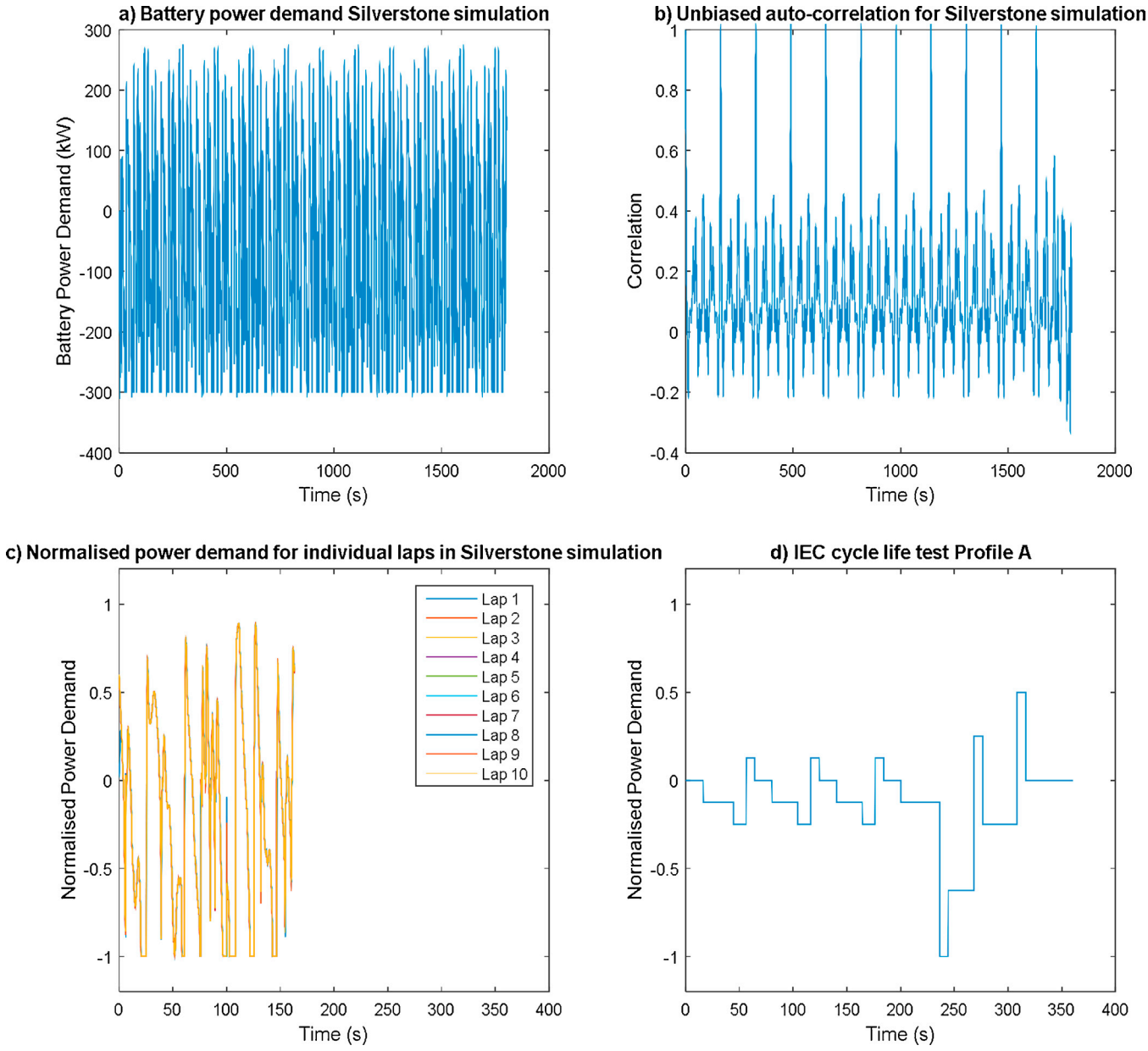

Fig. 2. Data Processing steps to produce individual Duty-cycles: a) Battery Power Demand as recorded for the simulation on Silverstone racing-circuit; b) Determination of period length using unbiased autocorrelation; c) Normalised power demand profile for individual laps on the Silverstone racing-circuit simulation; d) IEC 62660-1 cycle life test Profile A.

Table 4
Random pulse cycle target parameters.

No	Parameter (ζ)	Description (All power metrics refer to normalised values)	Value from database
1	P_{DC}	Mean duty-cycle discharge power	57.06%
2	P_C	Mean duty-cycle charge power	34.95%
3	P_{net}	Net duty-cycle discharge power	22.02%
4	P_{abs}	Mean duty-cycle absolute power	48.59%
5	κ_{DC}	% of time on discharge	61.6%
6	κ_C	% of time on charge	38.4%
7	τ_{AvgDC}	Mean discharge pulse duration	8.3s
8	τ_{maxDC}	Maximum discharge pulse duration	23.4s
9	τ_{AvgC}	Mean charge pulse duration	4.7s
10	τ_{maxC}	Maximum charge pulse duration	10.4s
11	T	Duration of the cycle	204.8s

$$\mathbb{D} = \{d_1(t), d_2(t), \ldots, d_j(t)\} \tag{8}$$

$$\mathbb{C} = \{c_1(t), c_2(t), \ldots, c_j(t)\} \tag{9}$$

The two subsets D and $\mathbb{C}$ can be further arranged into racing-circuit specific duty pulses as

$$\mathbb{D} = D_1 \cup D_2 \cup \ldots D_M \tag{10}$$

$$\mathbb{C} = C_1 \cup C_2 \cup \ldots C_M \tag{11}$$

where M ($M = 12$) is the number of racing-circuit duty-cycles in the database. Each subset (D_m, and C_m) contains the duty pulses $d_i^m(t)$ and $c_i^m(t)$, where m is the index for a specific racing-circuit and i is the index for a particular duty pulse.

$$D_m = \{d_1^m(t), d_2^m(t), \ldots, d_i^m(t)\} \tag{12}$$

$$C_m = \{c_1^m(t), c_2^m(t), \ldots, c_i^m(t)\} \tag{13}$$

The racing-circuits in this study produce a total of 189 charging and 189 discharging pulses.

Based on this knowledge the race circuit driving cycle database is analysed in terms of the parameters described in Table 4.

P_{DC} and P_C represent the average power sunk or sourced from the battery system during a duty-cycle. P_{net} is the net power demand that indicates how much power is demanded on average at every instant. P_{abs} defines the mean absolute power throughput describing how much power is either supplied to or demanded from the battery. κ_{DC} represents the fraction of time the battery is discharging. Conversely, κ_C is the fraction of time the battery is charging over the course of a duty-cycle. As the peak power demand for charging and discharging within this study is vehicle limited, the peak pulse amplitudes do not require an individual measure. These target parameters, collectively, describe the amount of energy supplied to and extracted from the system and the proportions in which this occurs.

The arithmetic mean and maximum duration of discharge pulses, τ_{AvgDC} and τ_{maxDC} are chosen to represent the shape and composition of the different discharge pulses. The target parameter for maximum pulse duration (τ_{maxDC}) ensures that a wide range of pulses are used and therefore the potential effects arising from prolonged high power demand are not excluded from the duty-cycle. Finally, the target duration of the duty-cycle (T) defines the length of one period of the test profile.

2.2.2. HP random pulse cycle

Using the target parameters from Table 4 in conjunction with the sets D and $\mathbb{C}$ it is possible to construct a representative duty-cycle using a process that extends the research described in [40,41]. The new method involves randomly selecting pairs of

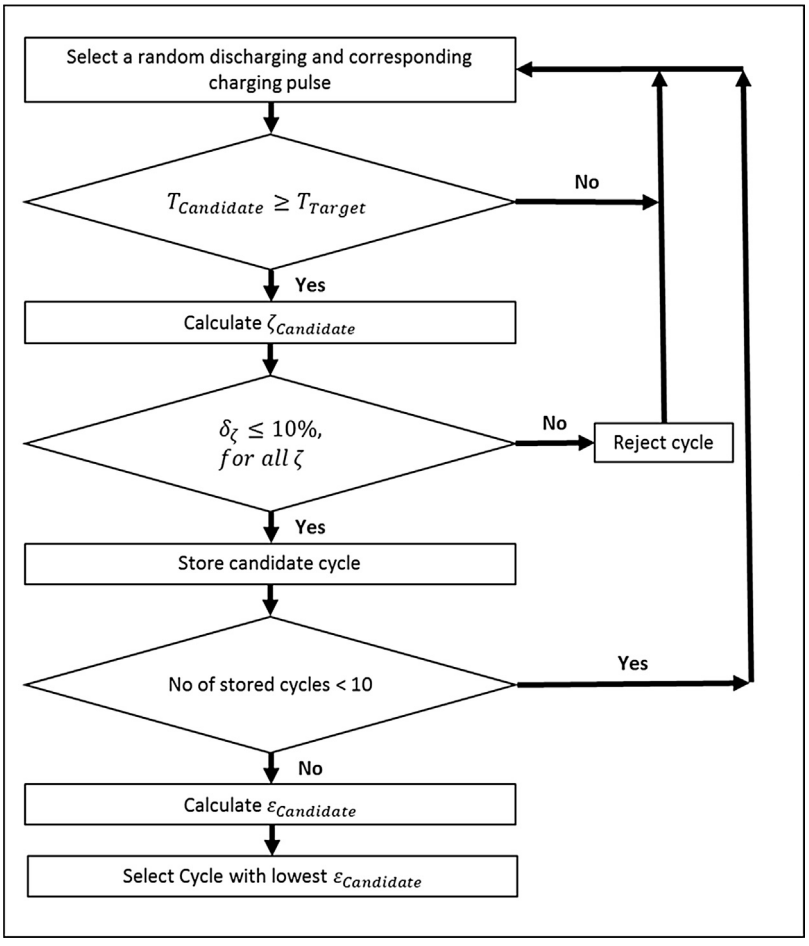

Fig. 3. Random pulse cycle (HP-RPC) construction methodology.

discharging and charging pulses and combining them to generate the complete HP duty-cycle. The resulting cycle is called a "HP Random Pulse Cycle" (HP-RPC). This process is illustrated in Fig. 3 and described in more detail below.

A uniform random number generator determines an integer index m with the condition $1 \leq m \leq 189$ for the sets D and $\mathbb{C}$. The indexed discharging pulse is selected from the set D followed by the charging pulse with the same index resulting in a duty-cycle as described in Eq. (14), where l is the number of generated indices.

$$R(t)_{Candidate} = [d_1, c_1, d_2, c_2, \ldots, d_l, c_l] \tag{14}$$

Selecting the charging pulse with the same index as the previous discharging pulse ensures a realistic sequence of charge and discharge pulses is created and avoids the occurrence of a short discharging pulse followed by a long charging pulse, which may not be possible within a real-world application since it results in a battery over-charge condition. This stage of the process is repeated and the pulses are concatenated until the target duration T is reached or exceeded as shown in Eq. (15). This resulting cycle is referred to as a *candidate cycle*.

$$T_{Candidate} \geq T_{Target} \tag{15}$$

The candidate cycle is subject to an assessment test to assess its suitability. Each of the eleven assessment parameters from Table 4 ($\zeta_{Candidate}$) are calculated for the candidate cycle ($\zeta_{Candidate}$). The error (δ_ζ) is calculated for eachζusing Eq. (16).

$$\delta_\zeta^{Candidate} = \left|\frac{\zeta_{Candidate} - \zeta_{target}}{\zeta_{target}}\right| \tag{16}$$

A cycle passes the assessment test if it fulfils the condition in Eq. (15) for each target parameter.

$$\delta_\zeta \leq 10\%, \quad \text{for all } \zeta \tag{17}$$

In [40,41] a cycle is only accepted as a candidate cycle if each of the assessment parameters is within a 5% error margin. Within this study however, a relaxation of the convergence criteria was required to ensure a candidate-cycle satisfied the criteria within an acceptable number of iterations. With δ_ζ set to 10%, it was found that 200 iterations of the process were required before suitable candidate cycles were identified. Conversely, with δ_ζ set to 5% more than 40,000 iterations failed to return an acceptable candidate cycle. The excessive computational time required with a reduced error margin was therefore deemed to reduce the usefulness of the method. It is noteworthy, that a larger database with greater variation of pulses may return a cycle that matches a more stringent selection criteria with a reduced number of iterations.

The evaluation process was repeated until 10 cycles were found that pass the assessment test. The cumulative error ($\varepsilon_{Candidate}$) is calculated as the sum of errors from $\delta_\zeta^{Candidate}$ for a particular candidate cycle as in Eq. (18), and the cycle with the smallest ($\varepsilon_{Candidate}$) is chosen as the HP-RPC.

$$\varepsilon_{\text{Candidate}} = \sum_\zeta \delta_\zeta^{\text{Candidate}} \tag{18}$$

2.3. Method two: HP multisine cycle

The second method of drive-cycle creation utilises the periodic nature of the HP duty-cycles as shown within Fig. 1a. Research presented within [24] describes a time-frequency domain swapping algorithm by which a signal is constructed which matches a user imposed amplitude spectrum ($f(f_k)$) in the

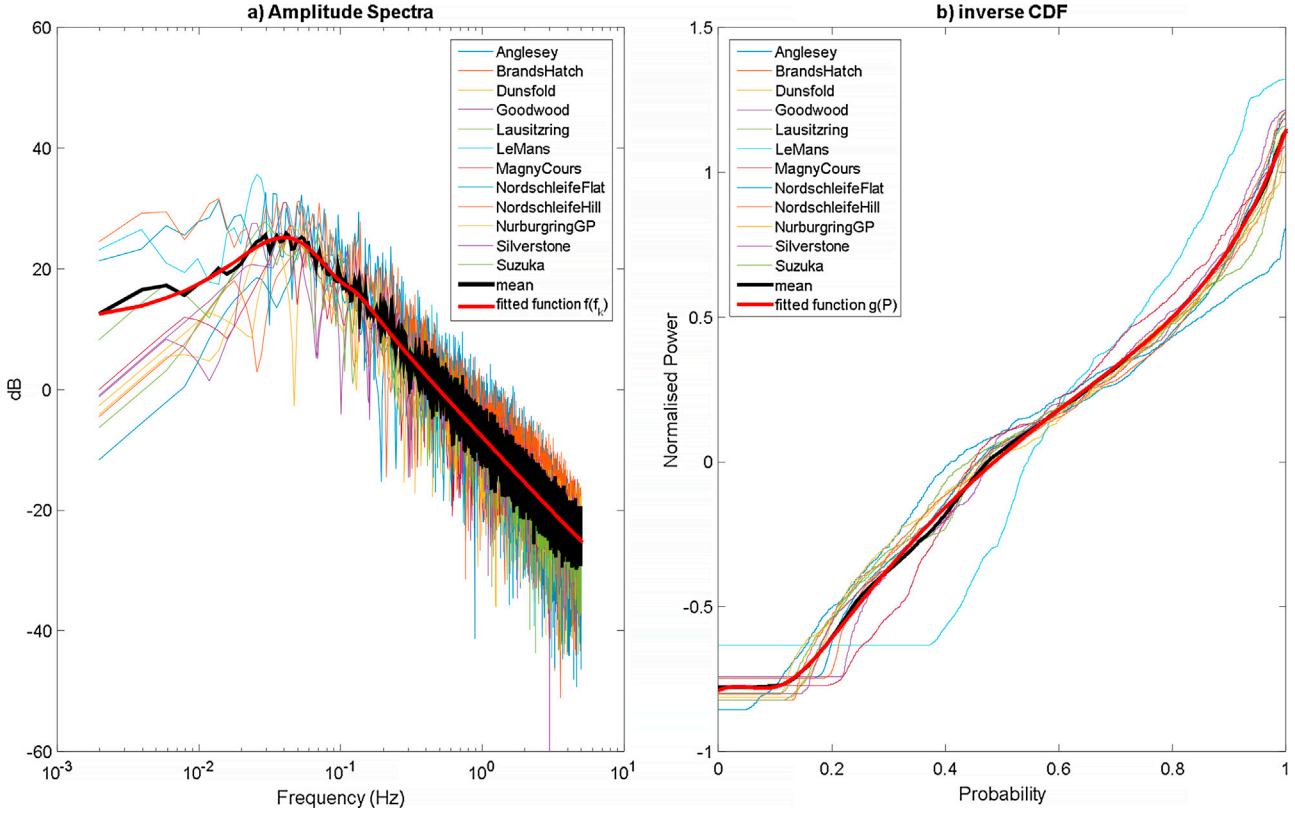

Fig. 4. a) amplitude spectra for average zero-mean laps; b) inverse CDF for average zero mean laps.

frequency domain and whose phases are optimised to match a desired inverse Cumulative Distribution Function (iCDF) ($g(P)$) in the time domain.

The amplitude spectrum of a signal $x(t)$ describes how much power the signal contains at the frequency f, and may be obtained via the Fourier series. The Fourier series of a time-based function $x(t)$ is defined in (19).

$$\mathrm{x}(n/f_s) = A_0 + \sum_{k=1}^{\infty} A_k \sin(2\pi n f_k + \phi_k) \tag{19}$$

A_k is the amplitude and φ_k is the phase of the k^{th} harmonic, f_k is the frequency at k^{th} harmonic and is $f_k = kf_s/N$ with f_s the sampling

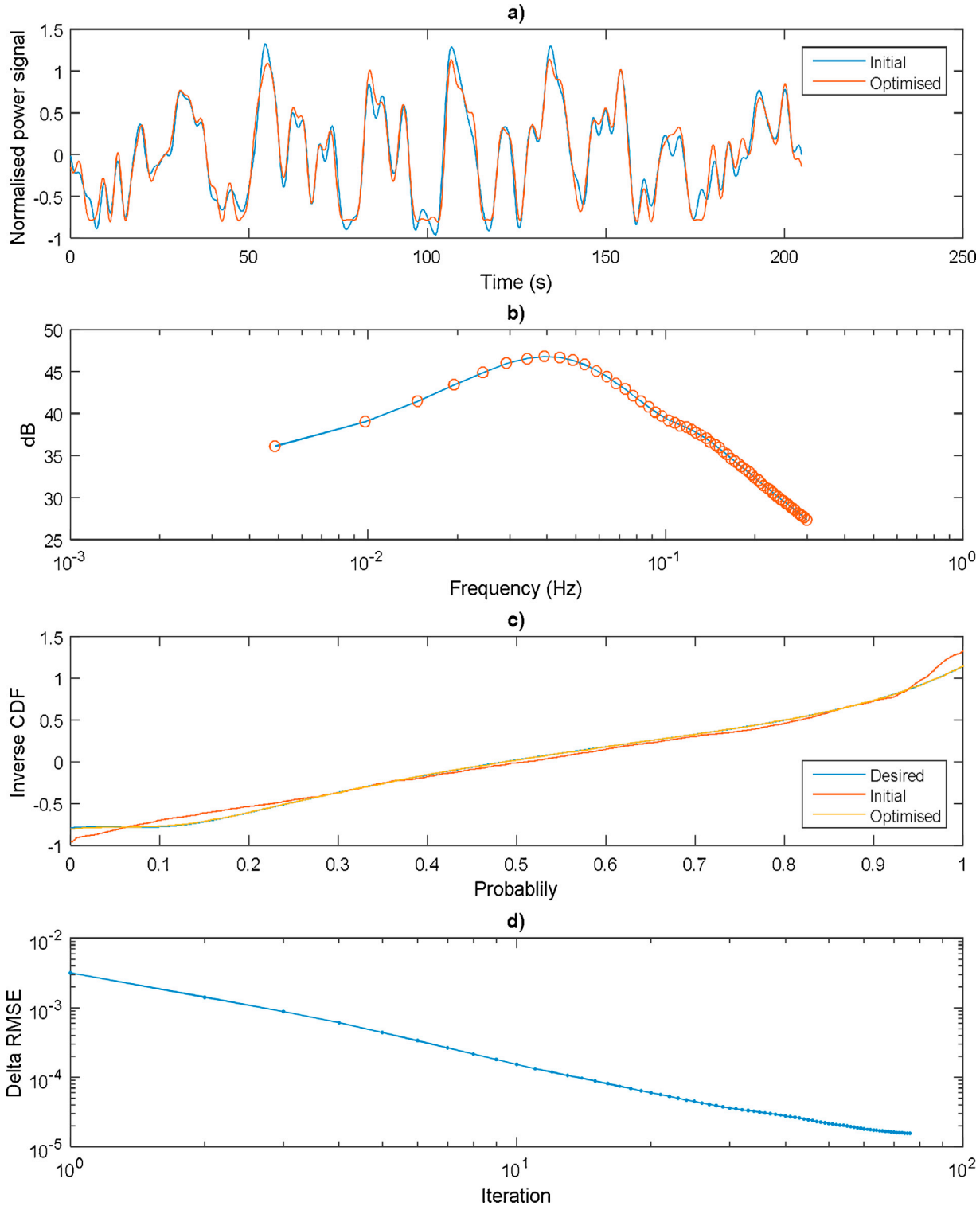

Fig. 5. Overview of Algorithm outcome a) A single period of the zero-mean Multisine Cycle; b) The amplitude spectrum up to 0.3 Hz; c) Desired, initial and optimised inverse cumulative distribution function; d) Progression of Power root mean squared error (RMSE).

frequency, and N is the number of samples per period. A detailed discussion into the derivation and use of Fourier Series for signal analysis is presented within a number of educational text, such as [47]. By performing a Fourier series, via the Fast Fourier Transform (FFT) routine for all duty-cycles in the database, the amplitudes and frequencies of the power demand pulses that a battery would be most subject to in HP driving are identified. From this, an amplitude spectrum that is representative of different HP scenarios within the frequency domain may be found. However, to produce a test-cycle that is also representative of the same HP scenarios in the time domain, knowledge of the associated phases are necessary which are selected via the time-frequency algorithm to match the desired iCDF

The Cumulative Distribution Function (CDF) for a quantity x that takes a real value at random is defined in Eq. (20). The right-hand term describes the probability that the random variable x has a value less than or equal to B. $F(B)$ is limited by boundaries of 0 and 1 and is non-decreasing.

$$F_x(B) = P[x \leq B] for B \in \mathbb{R} \tag{20}$$

Within a battery duty-cycle, if x is the amplitude of the power profile at a random point, then $F_x(B)$ is the probability that the amplitude of that operating point is equal to or less than B. For a profile with N data points the empirical cumulative distribution function (eCDF) is a step function increasing by 1/n at each data point. As such the eCDF is a measure for representation in the time domain, as it contains similar information to the target parameters associated with the random pulse method (see Table 4), except for the pulse duration (τ). The iCDF is simply the inverse of the eCDF and is shown in Eq. (21).

$$g(P) = F_x^{-1}(P) \tag{21}$$

As discussed within [24], a duty-cycle that matches an amplitude spectrum and iCDF associated with HP applications is therefore deemed to be representative within the frequency domain and the time domain.

2.3.1. Target criteria selection

The two main design criteria for the HP Multisine Cycle method are the amplitude spectrum and iCDF. The amplitude component at 0 Hz frequency (the DC component) can be ignored at the analysis stage and can be accounted for a later stage of the design. Therefore the mean (averaged over time) of each duty cycle in the racing circuit database is removed to construct a zero-mean duty-cycle database.

Fig. 4a) shows the amplitude spectra (in dB[1]) for each race circuit duty-cycle from the different racing-circuits presented in Section 2.1, as well as a function approximating the mean of the 12 duty-cycles. The values of the amplitude spectra lie within a certain band and all retain a similar shape with a broad spread of values at low frequencies converging to a narrower spread at higher frequencies. The mean spectrum lies within the band of spectra and follows the general shape and thus captures the characteristic in the frequency domain [25]. The mean amplitude spectrum here is approximated by a rational function $f(f_k)$ as expressed in Eq. (22).

$$\mathrm{f}(\mathrm{f_k}) = \frac{\sum \mathrm{a_i f_k^i}}{\sum \mathrm{c_i f_k^j}} \tag{22}$$

[1] $dB(x) = 20\log(x)$.

In this case the function most accurately representing the mean amplitude spectrum $f(f_k)$ (obtained by running a MATLAB curve fitting algorithm) is composed of a 4th order polynomial in the numerator and 5th order polynomial in the denominator.

Fig. 4b) shows the iCDF for each zero-mean duty-cycle in the database as well as the mean and a fitted function. The removal of the DC component results in a shift of the iCDF without influencing its shape. The functions all lie within a certain band and follow the same trend in terms of shape. An outlier in the results presented is the Le Mans racing-circuit (Table 3) duty-cycle. This circuit is known for long straights associated with extended high-power discharge pulses and fewer corners relating to fewer braking opportunities and thus fewer charging pulses. This makes the Le Mans racing-circuit a more extreme but not improbable scenario and as such it is not excluded from further analysis. The mean of the iCDF's is approximated by a rational function $g(P)$ as shown in Eq. (23). This forms the desired iCDF for the signal generation method.

$$\mathrm{g(P)} = \frac{\sum \mathrm{a_i P^i}}{\sum \mathrm{c_i P^j}} \tag{23}$$

The function best approaching the mean inverse CDF ($g(P)$) contains a 5th order polynomial in the numerator and 4th order polynomial in the denominator. The parameters for both the mean amplitude spectrum (Eq. (21)) and iCDF (Eq. (22)) functions are estimated using the Matlab function fitting toolbox. Out of the tested functions in Matlab, the rational function with the highest R^2 value and narrowest 95% confidence intervals for the coefficients was chosen.

2.3.2. HP multisine cycle

The progression of the implemented time-frequency swapping algorithm is illustrated in Fig. 5. The derivation and explanation of this algorithm is discussed within [24]. For completeness, a brief summary of the processing steps is outlined below.

The algorithm starts by generating a single period of a random phase multisine, which is a series of superimposed sinewaves with random phases (uniformly distributed between 0 and 2π), as defined in Eq. (24).

$$x(n) = \sum_{k=1}^{F} A_k \sin(2\pi n f_k + \phi_k) n = 0, 1, \ldots, N-1 \tag{24}$$

Again, f_k is the frequency at the k^{th} harmonic and is $f_k = kf_s/N$ with the sampling frequency f_s(assumed to be 10 Hz), N is the number of samples per period ($N = Tf_s$), where T is the period in seconds. For this duty-cycle T is set to the HP-RPC target of 204.8s, which in combination with the 10 Hz sampling rate results in 2048 samples. The amplitudes A_k for frequencies $f_k = \frac{f_s}{N}, \frac{2f_s}{N}, \ldots, F_{max}$ are determined from Eq. (25), where $F_{\max}$ denotes the highest frequency of interest.

$$A_k = f(f_k) \tag{25}$$

The function $f(f_k)$ approximates the mean amplitude spectrum as described in Eq. (22) and shown in Fig. 4a. It can also be seen in Fig. 4a that the majority of power in the amplitude spectrum is contained within the first 0.3 Hz. As such $F_{\max}$ is set to 0.3 Hz and a total of F amplitudes are determined for the first F frequencies where $F = \frac{F_{max}}{f_1}$. This produces the desired amplitude spectrum associated with the HP driving applications, as shown in Fig. 5b.

The phases φ_k for the F harmonics are initially chosen at random between 0 and 2π. Though the amplitude spectrum is matched, the random phases do not produce the desired iCDF (see Fig. 4c) for the initial random phase multisine signal (see Fig. 5a). The time-

frequency domain swapping algorithm enforces the desired iCDF ($g(P)$) and the desired amplitude spectrum ($f(f_k)$) iteratively until a convergence criterion is met as described below.

The sample values of the initial random phase multisine ($x_i(n)$, i denotes the iteration index) are sorted in ascending order and the indices of the values original position are recorded (Eq. (26)).

$$[y, \phi] = sort(x_i(n)). \tag{26}$$

These values of y are the iCDF of x_i (the zero-mean HP duty-cycle at the i^{th} iteration). The position variable (ϕ) serves as a timestamp indicating at which time in the duty-cycle the value y occurs. It can be seen in Fig. 5c) that the iCDF differs from the desired mean iCDF as described Eq. (23) in and shown in Fig. 4b).

To match the desired iCDF, a new duty-cycle ($y_i(n)$) is created by replacing each value in $x_i(n)$ with the corresponding value of $g(P)$ as in Eq. (27). The values for the desired iCDF ($g(P)$) are determined by using Eq. (23) for $P = \frac{1}{N}, \frac{2}{N}, \ldots, 1$.

$$y_i = sort^{-1}(g(P), \phi) \tag{27}$$

Eq. (27) implies that the smallest of the calculated values of $g(P)$ replaces the smallest value in $x_i(n)$, the second smallest value of $g(P)$ replaces the second smallest value in $x_i(t)$, and so forth. This process is repeated for all y resulting in a new duty-cycle with a changed amplitude spectrum and phases. The phases of this new duty-cycle are determined via the Discrete Fourier Transform and used to generate a new duty-cycle using the desired amplitude spectrum. This process is repeated, each time using the updated

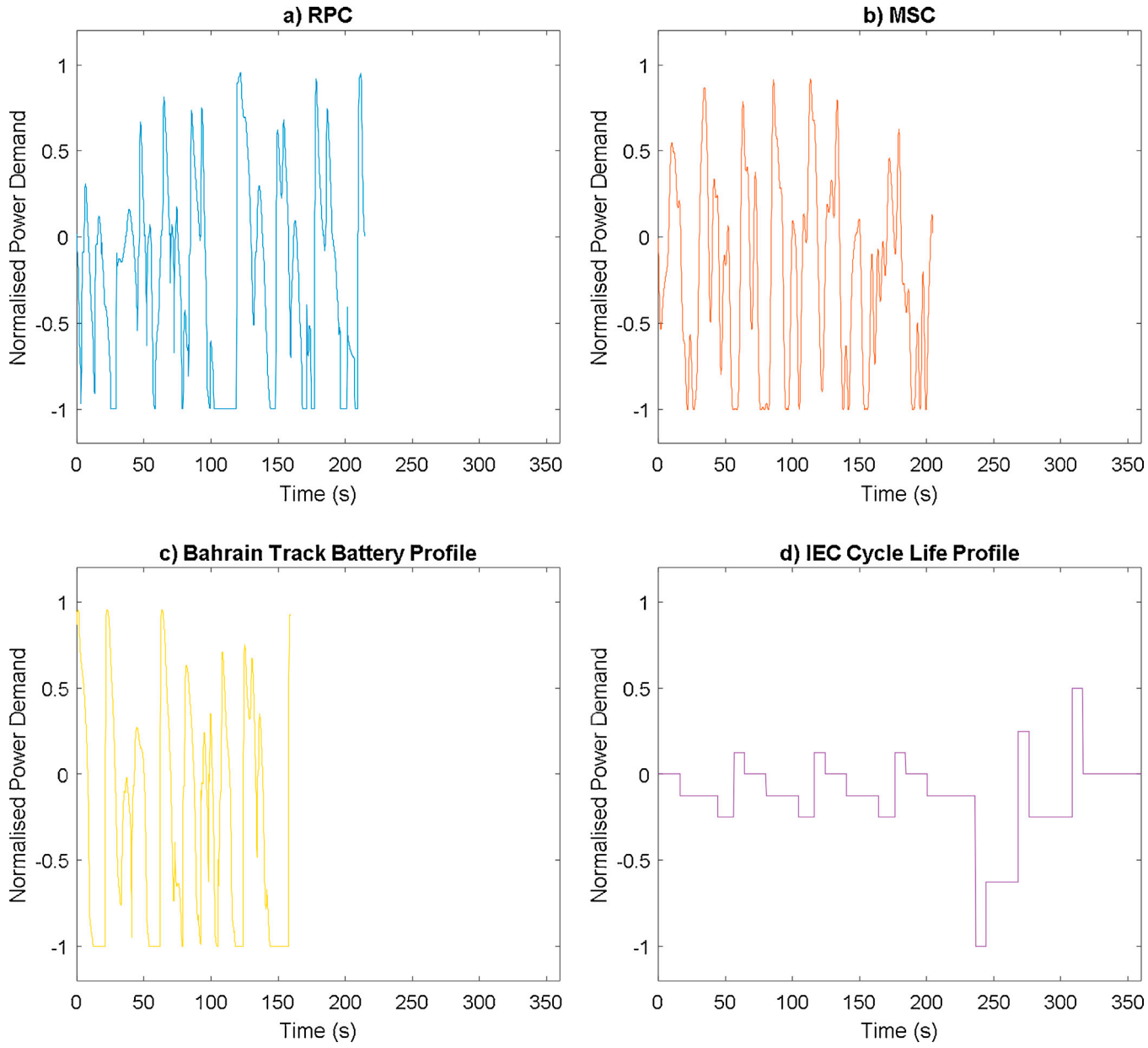

Fig. 6. a) Multisine Cycle; b) Random Pulse Cycle; c) Bahrain Racing-circuit simulation duty-cycle; d) IEC 62660-1 cycle life test profile A.

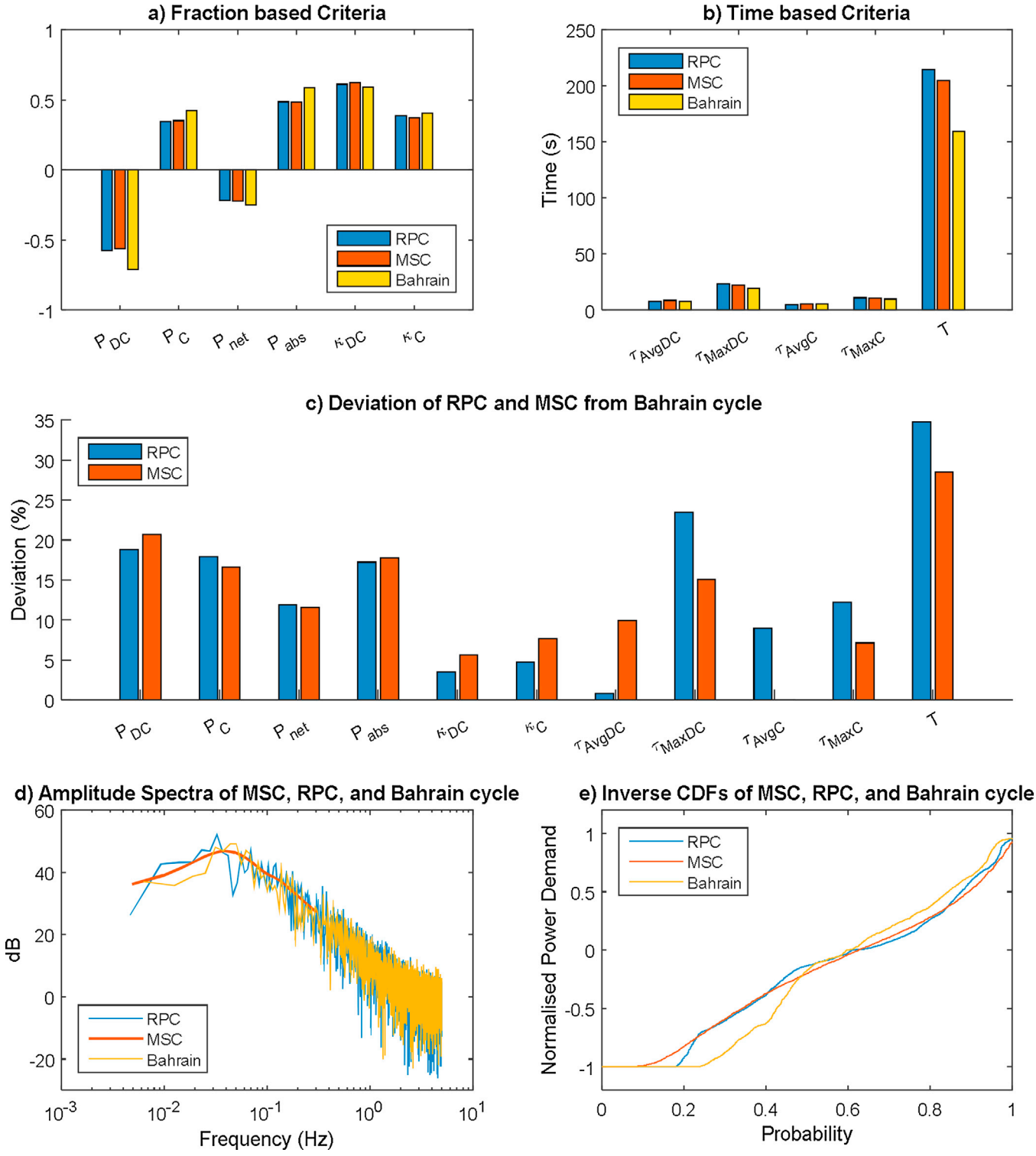

Fig. 7. Validation of HP-MSC and HP-RPC against the Bahrain cycle based on HP-RPC and HP-MSC design criteria. a) fraction based criteria; b) time based criteria; c) Deviation of HP-MSC & HP-RPC from Bahrain cycle based on HP-RPC criteria; d) Amplitude spectra for HP-RPC, HP-MSC and Bahrain; e) iCDF for HP-RPC,HP-MSC and Bahrain.

phases until a defined convergence between $sort(x_i(n))$ and $g(P)$ is met.

The convergence criteria chosen in this work is met if the change in the sum of errors between desired and optimised inverse CDF is smaller than 10^{-7}.The progression of this is shown in Fig. 5d, the resulting zero-mean cycle is shown in Fig. 5a. The HP Multisine Cycle (HP-MSC) is obtained once the mean DC component, synonymous with P_{net} in Table 4 is added. The final HP-MSC

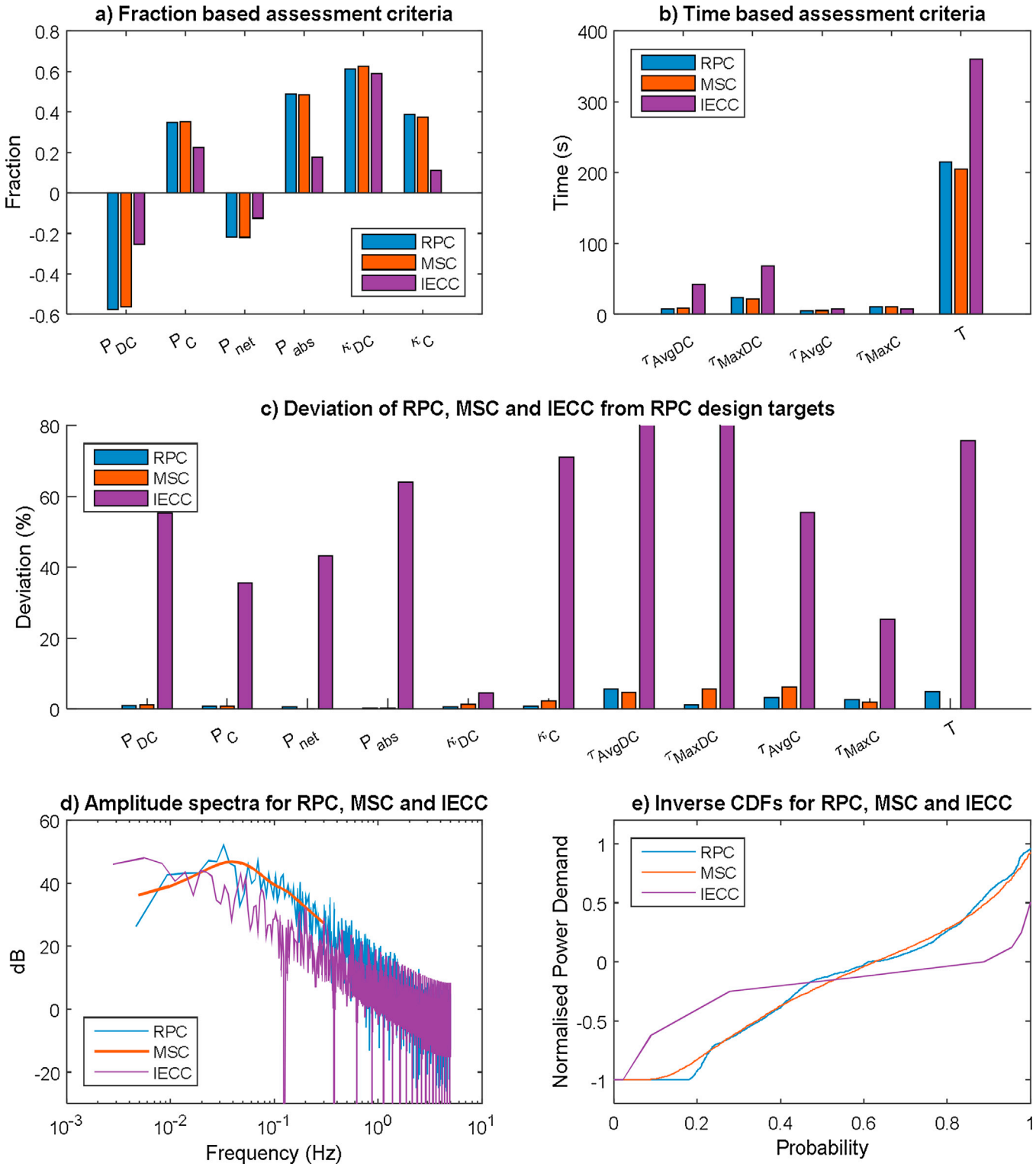

Fig. 8. Direct comparison between HP-RPC, HP-MSC and IECC in terms of a) fraction based criteria; b) time based criteria; c) Deviation of HP-RPC, HP-MSC and IECC from HP-RPC targets criteria; d) Amplitude spectra for HP-RPC, HP-MSC and IECC; e) iCDF for HP-RPC,HP-MSC and IECC.

contains instances where peak discharge demands exceed the −100% limit. This is attributed to the approximation of the mean iCDF by a function. Instances where the HP-MSC exceeds the discharging limit are constrained to −100%.

It is noteworthy that at the first instance, the profiles of $x(n)$ and $g(P)$ have different root mean square (RMS) values. For the algorithm to work it is necessary that the values of x_i after the initial iteration are adjusted to account for this using a correction

factor (fac_{rms}) as described in Eq. (28), and adjusting x_i as described in Eq. (29). The value of this correction factor is dependent on the frequency bandwidth of choice.

$$fac_{rms} = \frac{rms(g(P))}{rms(x(n))} \tag{28}$$

$$x(n) = x_i.fac_{rms} \tag{29}$$

3. Results

To verify the new duty-cycles that represent HP driving scenarios three different studies were undertaken. Firstly, the HP-MSC and HP-RPC are validated, using the assessment criteria for HP-RPC and HP-MSC, against a HP duty-cycle, which was not in the initial database of 12 race track duty cycles. This new HP duty cycle is the duty-cycle for the Bahrain International Circuit (Bahrain) and its generation followed the same methodology as the database duty-cycles. The modelled racing-circuit length is 5.439 km; which compares to the official length of 5.412 km resulting in an error of less than 0.5%.

Secondly, the HP-RPC and HP-MSC are compared to the IEC 62660-1 cycle life test profile A [6] (IECC) to further highlight the differences in these realisation of a HP duty-cycle compared with traditional and widely accepted test and characterisation cycles. The power-time traces of HP-RPC, HP-MSC, Bahrain, and IECC are shown in Fig. 6.

Finally, a thermal simulation study is undertaken for HP-RPC, HP-MSC, Bahrain, and IECC to estimate cell heating and the average volumetric temperature profile for a discharge from 100% to 10% SoC. As identified in the introduction, cell temperature is a main contributor to battery degradation and as such the self-heating of a cell during electrical loading should be considered as an influencing factor when considering cell degradation.

3.1. Validation of HP-MSC and HP-RPC

Fig. 7a and b show the design parameters, described in Table 4, calculated for HP-RPC, HP-MSC and the Bahrain duty-cycle. Despite the different methodologies applied to design each duty-cycle, the calculated parameters for HP-RPC and HP-MSC are very similar. Compared to the Bahrain cycle, a lower demand for mean discharge power (P_{DC}) and mean charge power (P_C) may be observed for both HP-RPC and HP-MSC. In turn, this results in corresponding lower values for net discharge power (P_{net}) and mean absolute power (P_{abs}). The difference between HP-RPC and the Bahrain cycle for these parameters range from 12.9% to 19.9%. Conversely, when comparing the HP-MSC and Bahrain circuit profile, the differences range from 11.6% to 20.7% respectively (see Fig. 7c). The percentage of time the battery is subjected to discharge (κ_{DC}) and subjected to charge (κ_{DC}) is similar between all cycles with differences of less than 8%.

Similar variations can be found for the time-based parameters, except for the maximum discharge pulse duration (τ_{MaxDC}) and cycle duration (T). Further analysis of the profiles, illustrated in Fig. 6a–c, reveals that the longest discharge pulse for the HP-RPC is 23.7 s compared to 22.1 s for the HP-MSC and 19.2 s for the Bahrain Cycle. The difference in peak pulse duration is small, in absolute terms, but amounts to 23.4% between Bahrain and HP-RPC, and 15.1% between Bahrain and HP-MSC.

Fig. 7d shows the amplitude spectra for the HP-RPC and Bahrain cycle up to 5 Hz and for the HP-MSC up to the design frequency of 0.3 Hz as presented in Section 2.3.1. The HP-MSC, HP-RPC and Bahrain cycle amplitude spectra follow the same general trend and as such all signals carry similar characteristics within the frequency domain. The flatness in peak power demand represented by the HP-RPC and Bahrain cycle is not captured in the HP-MSC. This observation is due to the exclusion of higher frequencies in the selection of the amplitude spectrum in the HP-MSC approach. Inclusion of higher frequencies (in the range of 0.3 Hz to 5 Hz) allows for a flattened peak demand for discharge pulses but also results in more frequent periods of charging and discharging. The performance of the HP-MSC against the time-based parameters in Fig. 7b may be adversely affected by fluctuations around zero amplitude, causing increased switching between charging and discharging. The performance of HP-MSC against target parameters, shown in Fig. 7a, and the cycle duration (T) remain unaffected by the inclusion of higher frequencies.

The iCDFs for all three cycles are displayed in Fig. 7e. They show that the discharge power demand for HP-RPC remains at peak power ($P < -0.9$) for 20.6% of the cycle duration compared to 16.7% for the HP-MSC and 29.2% for the Bahrain cycle. The proportion of power demand for discharging and charging, respectively, is similar between all cycles, an observation which is synonymous with the results presented in Fig. 7a–c.

3.2. Comparison between HP cycles and the IEC test standard

To highlight the difference between the realisation of a generic HP duty-cycle and a traditional automotive testing duty-cycle, HP-RPC and HP-MSC are compared to the cycle life test profile A (IECC) defined within the IEC 62660-1. The IECC contains only 8 s of peak discharging power demand per period compared to the previously identified 23.7 s for the HP-RPC and 22.1 s for the HP-MSC. In conjunction with a much longer period, this results in a very low value for the mean discharge power (P_{DC}) of 0.255. As shown in Fig. 8a, similar observations can be made for mean charge power P_C. As such, the values for net discharge power (P_{net})and mean absolute power (P_{abs}) also adopt much lower values for the IECC compared to the HP profiles. The percentage of time the battery is on discharge (κ_{DC}) is comparable between the HP cycles and standardised cycle. However, as the IECC contains resting periods at zero power demand and the HP profiles do not, their respective values for percentage of time the battery is on charge (κ_C) do not correlate.

The maximum and mean pulse duration for charging and discharging is shown in Fig. 8b and highlights further large differences. Although τ_{AvgDC} and τ_{MaxDC} indicate much longer

Table 5
Thermal simulation results for 20 Ah pouch cells.

Cycle	Duration (s)	Max. Temperature (°C)	Mean volumetric heat generation (kWm^{-3})	Mean heat generation (W)
HP-RPC	1491	44.0	107	28.3
HP-MSC	1530	43.9	106	27.9
Bahrain	1280	47.5	135	35.5
IECC	3121	30.0	30	7.9

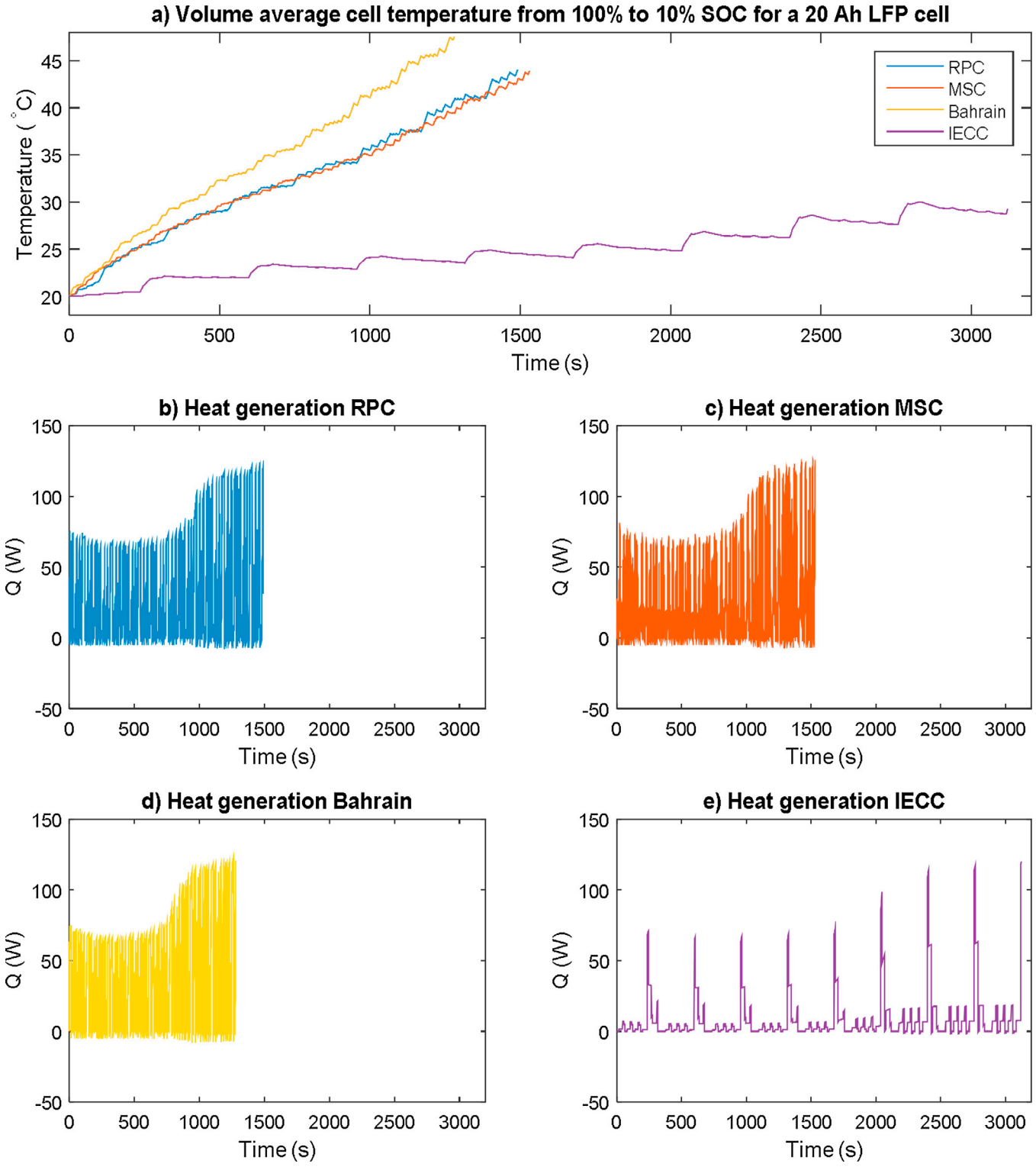

Fig. 9. a) Average cell temperature in degC during cycling from 100% – 10% SoC for a 20 Ah LFP cell; b) Cell heat generation for HP-RPC; c) Cell heat generation for HP-MSC; d) Cell heat generation for Bahrain; e) Cell heat generation for IECC.

individual discharging pulses for the IECC, the amplitude of the pulses is up to 70% lower and as such would result in much lower instantaneous heat generation. Assessing the deviation of HP-RPC, HP-MSC and IECC from the HP-RPC design targets as illustrated in Fig. 8c, reveals that the smallest deviation of the IECC from HP targets can be found for τ_{MaxC} at a value of 25.3% (except for κ_{DC}). Conversely, the largest deviation is for τ_{AvgDC} at a value of 410%.

As expected from a visual inspection of the cycles in Fig. 6, and the discrepancies between the different duty-cycles (HP-RPC, HP-MSC, and the IECC) shown in Fig. 8a–c, the amplitude spectra of

HP-RPC, HP-MSC and IECC (Fig. 8d) follow separate trends and as such the IECC is deemed not to be representative of HP driving scenarios within the frequency domain. Similarly, for the iCDFs in Fig. 8e, there is no identifiable correlation between these three cycles.

3.3. Thermal simulation study

To further illustrate the discrepancies between the IECC and HP duty-cycles, defined as part of this work and also to further highlight the correlation between the HP-RPC, HP-MSC and Bahrain cycle, a thermal simulation was undertaken to estimate the value of self-heating during a discharge from 100% to 10% SOC for each of the cycles.

A coupled 1D electrochemical-thermal model, developed through a complementary research activity within the University, was employed. The commercial software Comsol Multiphysics was employed for the numerical simulation. The validated thermal model was developed for a 20 Ah pouch cell, where the anode is made of graphite and the cathode material is lithium-iron-phosphate (LFP). The model has been validated at different C-rates, 0.5C, 1C, 3C, 5C and 10C under 20 °C ambient temperature. A complete discussion into the derivation of the model is presented within [48] and will not be repeated here.

During this simulation study, the maximum C-rate for charging was limited to 3C to comply with the manufacturer's specification for the cell. The maximum C-Rate for discharge was set at 8C, a value that resides within the validated range of the model. The ambient temperature of the simulation was set to 20 °C, and the heat transfer coefficient from the cell surface to the surroundings was defined as 10 $Wm^{-2}K^{-1}$ to emulate natural convection.

The results from this study are tabulated in Table 5 and presented in Fig. 9. The terms temperature and heat generation refer to the average volumetric temperature and average volumetric heat generation respectively within the cell.

Fig. 9a shows the volume average cell temperature for all four use cases. For HP cycles the maximum temperature is reached at the end of discharge. This translates to 1280s for the Bahrain cycle, 1491s for HP-RPC, and 1530 for HP-MSC and ranges from 43.9 °C to 47.5 °C. As the Bahrain cycle is more aggressive, as shown by Fig. 7a, than HP-RPC and HP-MSC respectively, the end of electrical loading is reached within a shorter time. In contrast, a cell undergoing the IECC schedule requires more than twice the time for the energy discharge to occur and reaches a peak temperature of only 30.0 °C.

The average cell volume heat generation for all four cycles is displayed in Fig. 9b–e. As expected the three HP cycles show a good correlation to each other. The highest recorded instance of heat generation is similar between all cycles to within 3%. However, the mean heat generation for the duration of the cycles varies significantly, with Bahrain displaying the highest heat generation term of 135 $kW.m^{-3}$. The mean heat generation for the IECC is of a lower order of magnitude at 30 $kW.m^{-3}$ resulting in a much lower temperature rise through electrical loading.

4. Discussion

4.1. Design of the HP duty-cycles

Two methods to design HP battery duty-cycles for cycle life and performance evaluation have been derived. The HP-RPC method extends a well-established technique from the literature for drive-cycle construction [40,41] by randomly selecting alternating charging and discharging power pulses. The target criteria that forms the cost function for cycle evaluation can be assessed to reflect the engineering challenge under investigation. Further, the relative error margins between each candidate cycle and the criteria can be selected by the engineer to optimise the inherent trade-off between computation time and cycle accuracy. For this research the error was set to 10% for each target criterion.

The second method evaluated for HP cycle definition follows a frequency-time swapping algorithm [24] to generate a cycle that matches a user defined amplitude spectrum and an inverse CDF. Both functions can be chosen by the design engineer, following the general criteria presented in Section 2.3.1. The choice of amplitude spectrum and CDF in this work are based on the mean of the spectra and CDFs within the HP duty-cycle database, representing different international race circuits. It has been shown that the HP-MSC method can be tuned to match the same targets as the HP-RPC by adaption of the iCDF. An advantage of this method is the relatively small amount of data required to generate a duty-cycle, as only the two design target functions are required, in contrast to an entire database of duty pulses.

4.2. Validation of the HP duty-cycles for the Bahrain international circuit

Validation of the cycles has shown a good degree of correlation between HP-RPC, HP-MSC and a cycle chosen at random from the database representing the Bahrain International Circuit. Although some differences such as power demand and time spent at peak have been observed, the results presented in Section 3.1 clearly show that the HP-MSC and HP-RPC offer a good approximation for this particular HP scenario with the average error between HP-RPC and HP-MSC compared with the Bahrain cycle of 14.0%, and 12.8% respectively. The amplitude spectra of all cycles follow a similar shape highlighting the similarity between the profiles. The iCDFs show clearly that the Bahrain cycle is more aggressive and demanding than the generic cycles. To cater for more demanding cycles, the database for HP-RPC may be expanded with further aggressive duty-cycles. For the HP-MSC generation method, an adjustment of the desired iCDF would be sufficient to tune the nature of the cycle to better represent this facet of the target HP duty-case.

Power demand and energy throughput for the Bahrain cycle are higher, but the longest pulse at peak power is smaller than that from the HP-RPC and HP-MSC. As shown in Fig. 9, this results in higher heat generation during electrical loading for the Bahrain cycle. The largest discrepancy between the cycles is the period (T) with a 34.8% deviation for HP-RPC and 28.5% deviation for HP-MSC. Arguably due to the repetitiveness of the pulses the shorter period of the Bahrain cycle by itself may be of lower significance to the profile as combined effects of τ_{MaxDC}, τ_{MaxC} and T are indirectly captured in the parameters P_{DC}, P_C, P_{net} and P_{abs}. The Bahrain cycle is only one particular scenario falling within the band of HP cycles, and as such, both HP-MSC and HP-RPC are deemed satisfactory to represent a typical HP cycle.

4.3. Comparison of the HP duty-cycles against standard test and characterisation cycles

The subsequent comparison of the HP scenarios with standardised tests shows large discrepancies between the cycles based on the HP-RPC and HP-MSC design criteria. This was confirmed by the thermal simulation study which showed much smaller peak temperatures and self-heating effects for the IECC compared to the HP cycles. As such, it can be concluded that there is too little commonality between the standard IECC and HP duty-cycles to warrant representation of the latter by the former.

5. Further work

The results presented within this paper have focused on the creation and application of a representative duty-cycle that may be employed to evaluate the integration of energy storage technology within a high-performance vehicle. The authors plan to extend the research presented within this work by conducting experimental tests investigating the thermal behavior of cells undergoing HP duty cycling and the rate and nature of degradation over prolonged HP use.

The methodologies presented are not limited to high-performance vehicles but provide a step by step guide for engineers and researchers to develop their own duty cycles for other industrial applications where standard testing procedures are not representative of real use. As discussed within a number studies [49,50], a representative duty-cycle underpins a range of engineering functions such as the component sizing; energy management; simulation and testing of the complete vehicle powertrain and key subsystems. As a result, the two methodologies presented are highly transferable to a number of different sectors that are investigating opportunities for electrification and the integration of battery systems. These include the electrification of marine and aerospace systems [51], either for more energy efficiency propulsion or because of the inclusion of more electrically powered ancillaries; in addition to the hybridization of off-highway or construction vehicles [52,53], where the diverse usage patterns prohibit the creation of a generic drive-cycle such as the NEDC or US06 that are common within the road transport sector.

The complete dataset of driving cycles and developed duty cycles is available from [54].

6. Conclusions

It may be concluded that both duty cycle construction methods presented within this research are suitable for the design of duty-cycles for battery performance evaluation within HP driving applications. Simulation results highlight that the new HP duty-cycles provide a more representative duty-cycle compared to traditional battery test standards. For high-performance vehicles, the ability to more accurately predict the performance requirements for the battery system within this emerging and strategically important emerging BEV sector will further support a range of engineering functions, such as the ability to optimise the energy capacity and power capability of the battery pack and to select and design the most appropriate thermal management strategy, further reducing system cost while concurrently increasing energy and power density. In addition, the ability to more accurately define the use-case for a HP-BEV will underpin ongoing experimentation and mathematical modelling to quantify the associated cell ageing and degradation that may occur within HP vehicle applications.

Acknowledgements

The research presented within this paper is supported by the Engineering and Physical Science Research Council (EPSRC-EP/M507593/1) and (ELEVATE- EP/M009394/1). The research was undertaken in collaboration with the WMG Centre High Value Manufacturing Catapult (funded by Innovate UK) in collaboration with Jaguar Land Rover and Delta Motorsport. The authors would like to express gratitude to Paul Haney, Nigel Taylor and Limhi Somerville from Jaguar Land Rover and Nick Carpenter from Delta Motorsport for their advice and support.

References

[1] E.-H. Aglzim, Z. Asus, D. Chrenko, Z.H. Che Daud, L. Le Moyne, Dynamic modeling and driving cycle prediction for a racing series hybrid car, IEEE J. Emerg. Sel. Top. Power Electron. 6777 (2014) 1, doi:http://dx.doi.org/10.1109/JESTPE.2014.2307079.
[2] D. Asus, E. Chrenko, A. Aglzim, A. Kebairi, L. Keromnes, Model and control strategy simulation of a racing series hybrid car, 2014 IEEE Veh. Power Propuls. Conf., IEEE (2014) 1–6, doi:http://dx.doi.org/10.1109/VPPC.2014.7007100.
[3] A. Devie, E. Vinot, S. Pelissier, P. Venet, Real-world battery duty profile of a neighbourhood electric vehicle, Transp. Res. C Emerg. Technol. 25 (2012) 122–133, doi:http://dx.doi.org/10.1016/j.trc.2012.05.003.
[4] B.Y. Liaw, M. Dubarry, From driving cycle analysis to understanding battery performance in real-life electric hybrid vehicle operation, J. Power Sources 174 (2007) 76–88, doi:http://dx.doi.org/10.1016/j.jpowsour.2007.06.010.
[5] Idaho National Laboratory (INL), Plugged In: How Americans Charge Their Electric Vehicles, 2015.
[6] International Electrotechnical Commission, IEC 62660-1, 2010.
[7] BSI Standards Publication (2012), BS ISO 12405-2:2012 Electrically propelled road vehicles—Test specification for lithium-ion traction battery packs and systems, 2012.
[8] Idaho National Laboratory, U.S. Department of Energy Vehicle Technologies Program Battery Test Manual For Plug-In Hybrid Electric Vehicles – Revision 3, U.S. Dep. Energy, 2015, 16–18.
[9] E.C. Castillo, Standards for Electric Vehicle Batteries and Associated Testing Procedures, Elsevier Ltd., 2015, doi:http://dx.doi.org/10.1016/B978-1-78242-377-5.00018-2.
[10] J. Lin, D.A. Niemeier, Estimating regional air quality vehicle emission inventories: constructing robust driving cycles, Transp. Sci. 37 (2003) 330, doi:http://dx.doi.org/10.1108/17506200710779521.
[11] J. Lin, D.A. Niemeier, An exploratory analysis comparing a stochastic driving cycle to California's regulatory cycle, Atmos. Environ. 36 (2002) 5759–5770, doi:http://dx.doi.org/10.1016/S1352-2310(02)00695-7.
[12] M.R. Palacín, Recent advances in rechargeable battery materials: a chemist's perspective, Chem. Soc. Rev. 38 (2009) 2565–2575, doi:http://dx.doi.org/10.1039/b820555h.
[13] J. Vetter, P. Novák, M.R. Wagner, C. Veit, K.-C. Möller, J.O. Besenhard, M. Winter, M. Wohlfahrt-Mehrens, C. Vogler, A. Hammouche, Ageing Mechanisms in lithium-ion batteries, J. Power Sources 147 (2005) 269–281, doi:http://dx.doi.org/10.1016/j.jpowsour.2005.01.006.
[14] A. Barré, B. Deguilhem, S. Grolleau, M. Gérard, F. Suard, D. Riu, A review on lithium-ion battery ageing mechanisms and estimations for automotive applications, J. Power Sources 241 (2013) 680–689, doi:http://dx.doi.org/10.1016/j.jpowsour.2013.05.040Review.
[15] M. Wohlfahrt-Mehrens, C. Vogler, J. Garche, Aging mechanisms of lithium cathode materials, J. Power Sources 127 (2004) 58–64, doi:http://dx.doi.org/10.1016/j.jpowsour.2003.09.034.
[16] T. Waldmann, M. Wilka, M. Kasper, M. Fleischhammer, M. Wohlfahrt-Mehrens, Temperature dependent ageing mechanisms in Lithium-ion batteries – a post-mortem study, J. Power Sources 262 (2014) 129–135, doi:http://dx.doi.org/10.1016/j.jpowsour.2014.03.112.
[17] K. Uddin, S. Perera, W. Widanage, L. Somerville, J. Marco, Characterising lithium-Ion battery degradation through the identification and tracking of electrochemical battery model parameters, Batteries 2 (2016) 13, doi:http://dx.doi.org/10.3390/batteries2020013.
[18] L.E. Downie, L.J. Krause, J.C. Burns, L.D. Jensen, V.L. Chevrier, J.R. Dahn, In situ detection of lithium plating on graphite electrodes by electrochemical calorimetry, J. Electrochem. Soc. 160 (2013) A588–A594, doi:http://dx.doi.org/10.1149/2.049304jes.
[19] M.S.D. Darma, M. Lang, K. Kleiner, L. Mereacre, V. Liebau, F. Fauth, T. Bergfeldt, H. Ehrenberg, The influence of cycling temperature and cycling rate on the phase specific degradation of a positive electrode in lithium ion batteries: a post mortem analysis, J. Power Sources 327 (2016) 714–725, doi:http://dx.doi.org/10.1016/j.jpowsour.2016.07.115.
[20] M, M.S.D. Lang, K. Darma, L. Kleiner, L. Riekehr, Mereacre, V. Ávila Pérez, H. Liebau, Post mortem analysis of fatigue mechanisms in LiNi 0.8 co 0.15 Al 0.05 o 2–LiNi 0.5 Co 0. 2ÁMn 0.3 o 2–LiMn 2 O 4/graphite lithium ion batteries, J. Power Sources 326 (2016) 397–409, doi:http://dx.doi.org/10.1016/j.jpowsour.2016.07.010.
[21] R. Kostecki, F. McLarnon, Microprobe study of the effect of Li intercalation on the structure of graphite, J. Power Sources 119–121 (2003) 550–554, doi:http://dx.doi.org/10.1016/S0378-7753(03)00287-8.
[22] M. Broussely, P. Biensan, F. Bonhomme, P. Blanchard, S. Herreyre, K. Nechev, R.J. Staniewicz, Main aging mechanisms in Li ion batteries, J. Power Sources 146 (2005) 90–96, doi:http://dx.doi.org/10.1016/j.jpowsour.2005.03.172.
[23] G. Sarre, P. Blanchard, M. Broussely, Aging of lithium-ion batteries, J. Power Sources 127 (2004) 65–71, doi:http://dx.doi.org/10.1016/j.jpowsour.2003.09.008.
[24] J. Schoukens, T. Dobrowiecki, Design of broadband excitation signals with a user imposed power spectrum and amplitude distribution, IEEE Instrum. Meas. Technol. Conf. (1998) 1002–1005.
[25] W.D. Widanage, A., Barai, K., Uddin, A., Mcgordon, J. Marco, Design and use of multisine signals for Li-ion battery equivalent circuit modelling. Part 1: Signal design, Submitt. to J. Power Sources (under Rev. 324 (2015) 1–25. 10.1016/j.jpowsour.2016.05.014.

[26] W.D. Widanage, A. Barai, G.H. Chouchelamane, K. Uddin, A. McGordon, J. Marco, P. Jennings, Design and use of multisine signals for Li-ion battery equivalent circuit modelling. Part 2: model estimation, J. Power Sources 324 (2016) 61–69, doi:http://dx.doi.org/10.1016/j.jpowsour.2016.05.014.
[27] Q. Kellner, W. Dhammika Widanage, J. Marco, Battery power requirements in high-performance electric vehicles, 2016 IEEE Transp. Electrif. Conf. Expo, IEEE, Dearborn MI, USA, 2016, pp. 1–6, doi:http://dx.doi.org/10.1109/ITEC.2016.7520194.
[28] IPG Automotive GmbH, IPG CarMaker User's Guide (v4.5.5), 2014.
[29] IPG Automotive GmbH, IPGDriver User Manual 6.4, 2014, 1–153.
[30] IPG Automotive GmbH, CarMaker Reference Manual V. 5.1, 2014.
[31] Robert Bosch GmbH, Bosch Automotive Handbook, 7th ed., SAE, Plochingen, 2007.
[32] J.Y. Stein, Digital Signal Processing: A Computer Science Perspective, John Wiley & Sons Ltd., 2000.
[33] T.J. Lyons, J.R. Kenworthy, P.I. Austin, P.W.G. Newman, The development of a driving cycle for fuel consumption and emissions evaluation, Transp. Res. A Gen. 20 (1986) 447–462, doi:http://dx.doi.org/10.1016/0191-2607(86)90081-6.
[34] M. André, The ARTEMIS European driving cycles for measuring car pollutant emissions, Sci. Total Environ. 334–335 (2004) 73–84, doi:http://dx.doi.org/10.1016/j.scitotenv.2004.04.070.
[35] W.T. Hung, K.M. Tam, C.P. Lee, L.Y. Chan, C.S. Cheung, Comparison of driving characteristics in cities of Pearl River Delta, China, Atmos. Environ. 39 (2005) 615–625, doi:http://dx.doi.org/10.1016/j.atmosenv.2004.10.019.
[36] S.H. Kamble, T.V. Mathew, G.K. Sharma, Development of real-world driving cycle: case study of Pune, India, Transp. Res. D Transp. Environ. 14 (2009) 132–140, doi:http://dx.doi.org/10.1016/j.trd.2008.11.008.
[37] S.H. Ho, Y.D. Wong, V.W.C. Chang, Developing Singapore Driving Cycle for passenger cars to estimate fuel consumption and vehicular emissions, Atmos. Environ. 97 (2014) 353–362, doi:http://dx.doi.org/10.1016/j.atmosenv.2014.08.042.
[38] J.H.H. Kent, G.H.H. Allen, G. Rule, A driving cycle for Sydney, Transp. Res. 12 (1978) 147–152, doi:http://dx.doi.org/10.1016/0041-1647(78)90117-X.
[39] J. Liu, X. Wang, A. Khattak, Customizing driving cycles to support vehicle purchase and use decisions: fuel economy estimation for alternative fuel vehicle users, Transp. Res. C Emerg. Technol. 67 (2016) 280–298, doi:http://dx.doi.org/10.1016/j.trc.2016.02.016.
[40] H.Y.Y. Tong, W.T.T. Hung, C.S.S. Cheung, Development of a driving cycle for Hong Kong, Atmos. Environ. 33 (1999) 2323–2335, doi:http://dx.doi.org/10.1016/S1352-2310(99)00074-6.
[41] W.T. Hung, H.Y. Tong, C.P. Lee, K. Ha, L.Y. Pao, Development of a practical driving cycle construction methodology: a case study in Hong Kong, Transp. Res. D Transp. Environ. 12 (2007) 115–128, doi:http://dx.doi.org/10.1016/j.trd.2007.01.002.
[42] J. Groot, M. Swierczynski, A.I. Stan, S.K. Kær, On the complex ageing characteristics of high-power LiFePO4/graphite battery cells cycled with high charge and discharge currents, J. Power Sources 286 (2015) 475–487, doi:http://dx.doi.org/10.1016/j.jpowsour.2015.04.001.
[43] M. Dubarry, C. Truchot, M. Cugnet, B.Y. Liaw, K. Gering, S. Sazhin, D. Jamison, C. Michelbacher, Evaluation of commercial lithium-ion cells based on composite positive electrode for plug-in hybrid electric vehicle applications. Part I: initial characterizations, J. Power Sources 196 (2011) 10328–10335, doi:http://dx.doi.org/10.1016/j.jpowsour.2011.08.077.
[44] K.L. Gering, S.V. Sazhin, D.K. Jamison, C.J. Michelbacher, B.Y. Liaw, M. Dubarry, M. Cugnet, Investigation of path dependence in commercial lithium-ion cells chosen for plug-in hybrid vehicle duty cycle protocols, J. Power Sources 196 (2011) 3395–3403, doi:http://dx.doi.org/10.1016/j.jpowsour.2010.05.058.
[45] D. Wong, B. Shrestha, D.A. Wetz, J.M. Heinzel, Impact of high rate discharge on the aging of lithium nickel cobalt aluminum oxide batteries, J. Power Sources 280 (2015) 363–372, doi:http://dx.doi.org/10.1016/j.jpowsour.2015.01.110.
[46] J. Lin, D.A. Niemeier, Regional driving characteristics, regional driving cycles, Transp. Res. D Transp. Environ. 8 (2003) 361–381, doi:http://dx.doi.org/10.1016/S1361-9209(03)00022-1.
[47] A. Croft, R. Davidson, Mathematics for Engineers, 3rd edition, Pearson Education Limited, Essex, England, 2008.
[48] D. Worwood, E., Hosseinzadeh, Q., Kellner, J., Marco, D., Greenwood, W., McGlen, R., W. Dhammika, A., Barai, P.A. (Paul A. Jennings, Thermal analysis of a lithium-ion pouch cell under aggressive automotive duty cycles with minimal cooling, in: IET Hybrid Electr. Veh. Conf., 2016: pp. 2–3.
[49] A. Fröberg, L. Nielsen, Efficient drive cycle simulation, IEEE Trans. Veh. Technol. 57 (2008) 1442–1453, doi:http://dx.doi.org/10.1109/TVT.2007.907310.
[50] A.I. Antoniou, J. Komyathy, J. Bench, A. Emadi, Modeling and simulation of various hybrid-electric configurations of the high-mobility multipurpose wheeled vehicle (HMMWV), IEEE Trans. Veh. Technol. 56 (2007) 459–465, doi:http://dx.doi.org/10.1109/TVT.2007.891490.
[51] H. Lan, S. Wen, Y.Y. Hong, D.C. Yu, L. Zhang, Optimal sizing of hybrid PV/diesel/battery in ship power system, Appl. Energy. 158 (2015) 26–34, doi:http://dx.doi.org/10.1016/j.apenergy.2015.08.031.
[52] T.Q. Dinh, J. Marco, H. Niu, D. Greenwood, L. Harper, D. Corrochano, A novel method for idle-stop-start control of micro hybrid construction equipment—part A: fundamental concepts and design, Energies 10 (2017) 962, doi:http://dx.doi.org/10.3390/en10070962.
[53] T. Dinh, J. Marco, H. Niu, D. Greenwood, L. Harper, D. Corrochano, A novel method for idle-stop-start control of micro hybrid construction equipment—part B: a real-Time comparative study, Energies 10 (2017) 1250, doi:http://dx.doi.org/10.3390/en10091250.
[54] [dataset] [54] Q. Kellner, Drive and duty cycle database, 2017. http://wrap.warwick.ac.uk/94878.